

Thermoradiative Device Enhanced by Near-field Coupled Structures

Wang, B.; Lin, C.; Teo, K.H.; Zhang, Z.

TR2017-048 July 2017

Abstract

Thermoradiative (TR) technology was recently proposed as a new mechanism to efficiently convert low-temperature waste heat into electric energy. It has been shown that near-field coupling between a TR cell and a heat sink is an effective way in boosting the performance of the TR device. The enhancement becomes more significant when surface resonant modes are supported by the heat sink. Surface plasmon polaritons on metal surfaces, and surface phonon polaritons on Lorentz materials, are two major types of materials investigated in the near-field enhancement. However, to significantly boost the performance, the resonant mode energy needs to match the bandgap energy of the TR cell, which is often difficult to realize with natural material selections. Typical metals have plasma frequency much higher than the bandgap of TR cell. In this paper, we show that new resonant modes with energy close to the bandgap of TR cell can be created with nanostructured gratings on the heat sink. This enables use to build the heat sink using commonly available metallic materials, whose typical surface resonant frequency is much higher than the TR bandgap.

Journal of Quantitative Spectroscopy & Radiative Transfer

This work may not be copied or reproduced in whole or in part for any commercial purpose. Permission to copy in whole or in part without payment of fee is granted for nonprofit educational and research purposes provided that all such whole or partial copies include the following: a notice that such copying is by permission of Mitsubishi Electric Research Laboratories, Inc.; an acknowledgment of the authors and individual contributions to the work; and all applicable portions of the copyright notice. Copying, reproduction, or republishing for any other purpose shall require a license with payment of fee to Mitsubishi Electric Research Laboratories, Inc. All rights reserved.

Thermoradiative Device Enhanced by Near-field Coupled Structures

Bingnan Wang,¹ Chungwei Lin,¹ Koon Hoo Teo,¹ and Zhuomin Zhang²

¹Mitsubishi Electric Research Laboratories,

201 Broadway Ste 8, Cambridge, MA 02139 USA

²George W. Woodruff School of Mechanical Engineering,

Georgia Institute of Technology, Atlanta, GA 30332, USA

Abstract

Thermoradiative (TR) technology was recently proposed as a new mechanism to efficiently convert low-temperature waste heat into electric energy. It has been shown that near-field coupling between a TR cell and a heat sink is an effective way in boosting the performance of the TR device. The enhancement becomes more significant when surface resonant modes are supported by the heat sink. Surface plasmon polaritons on metal surfaces, and surface phonon polaritons on Lorentz materials, are two major types of materials investigated in the near-field enhancement. However, to significantly boost the performance, the resonant mode energy needs to match the bandgap energy of the TR cell, which is often difficult to realize with natural material selections. Typical metals have plasma frequency much higher than the bandgap of TR cell. In this paper, we show that new resonant modes with energy close to the bandgap of TR cell can be created with nanostructured gratings on the heat sink. This enables use to build the heat sink using commonly available metallic materials, whose typical surface resonant frequency is much higher than the TR bandgap.

INTRODUCTION

Recently, thermoradiative (TR) cells have been proposed as heat engines to convert heat into electricity [1–4]. The simplest form of a TR cell consists of a p-n junction that is heated to a higher temperature T_c than ambient T_a . In Ref. [1], the working principle of the TR cell was proposed, and the fundamental limit of its power conversion efficiency was analyzed using the Shockley-Queisser framework (i.e. assuming the blackbody spectrum and including the radiative combination only). The concept was demonstrated by experiments [3], although the realized efficiency was low. It is possible to boost the efficiency by designing the TR cell with nanophotonic approaches, which have been widely explored for photovoltaic (PV) and thermophotovoltaic (TPV) cells [5–8], such that selective radiation at a narrow band just above the bandgap energy is achieved. However, in this case the radiation power would be greatly suppressed. As a result, the generated power density would be extremely small [9].

However, with near-field resonant coupling, the radiation can go beyond the blackbody limit, and all the radiation power can be “squeezed” into a narrow bandwidth around the resonance [10]. Based on this understanding, in Ref. [4], a heat sink was placed in close vicinity of the TR cell. It was shown that by near-field coupling of the photons generated from the TR cell to the phonon polariton mode that is supported on the surface of the heat sink (whose dispersion is described by a Lorentz model), both the conversion efficiency and the generated power density can be greatly enhanced when the resonance is very close to the bandgap energy of the TR cell. In Ref. [11], the near-field enhancement effect of TR cells was further explored, and it was shown that a metallic material, whose dispersion is described by a Drude model and supports surface plasmon polaritons

(SPPs), is also good candidate for heat sink, and can have an even more significant output power density enhancement effect as compared with Lorentz type materials. The enhancement effect was understood from the impedance matching condition derived from coupled-mode theory [10, 12–15]. In the case of radiative energy transfer dominated by resonant coupling between two objects (TR cell and the heat sink, in the case of TR device), the transfer is maximized when the resonance decays into the two objects at the same rate. This condition is easier to achieve with a Drude type metallic material. An additional advantage with metals as heat sink is their typically larger thermal conductivities compared with insulators. The faster heat dissipation makes it easier to maintain a temperature close to the ambient.

To use TR cell based devices to harvest low-grade waste heat with temperature of 1000 K or lower, the preferred band gap energy of TR cell is 0.3 eV or lower [1]. In order for the near-field resonant coupling to work, the resonant mode needs to have an energy slightly above the band gap energy of the cell. However, typical noble metals have surface plasmon resonance with much higher energy [16]. For example, plasma frequency ω_p of gold is around 9 eV, and the frequency of SPP on planar gold surface $\omega_{SPP} = \omega_p / \sqrt{2}$ is around 6.4 eV, which is more than 20 times higher than the typical TR cell band gap energy.

In this paper, we show that this huge difference can be compensated via adding nanostructured patterns on the heat sink. In particular, we show that the periodic grating structures introduce additional surface resonance modes whose energies are much lower than SPP modes, and are much closer to the band gap energy of the TR cell. Depending on the material and geometrical parameters of the grating, different resonant modes can be utilized, such as localized SPPs, waveguide modes, and spoof polaritons [17]. With two different grating configurations, we show that different

metallic materials including typical noble metals can be used as heat sink to enhance the radiative heat transfer and boost the output power density and conversion efficiency of the TR cell.

TR DEVICE PRINCIPLE AND MODEL

We first briefly summarize the working principle of a TR cell. For a semiconductor diode at temperature T_c exchanging energy via radiation of photons with a thermal reservoir (either a heat source or a heat sink) at temperature T_a , the photon emission and absorption are due to transitions across the band gap and are associated with electron-hole (e-h) pair recombination and generation, respectively [1, 9, 11]. When $T_c = T_a$, the emitted photon flux from the cell is the same as the photon flux absorbed by it, and the e-h population is in equilibrium determined by T_c , meaning no current can be generated when an external load is connected to the cell. When $T_c \neq T_a$, there will be an imbalance in photon emission and absorption, leading to a splitting of quasi-Fermi levels, $\Delta\mu$, of electrons and holes.

In the case of TR cell, $T_c > T_a$, the emitted photon flux is larger than the absorbed photon flux, and the e-h population becomes smaller than the equilibrium at T_c . As a result, the cell tends to get back to the equilibrium by generating e-h pairs via all possible channels. Because of this tendency, when connected to an external load, the cell will transfer electrons in the valence band to conduction band through the load, effectively generating an electric current. In comparison, a PV cell has $T_c < T_a$, absorbs more photons than it emits, and accumulates more e-h pairs than the equilibrium state, therefore has a tendency to recombine the excess e-h pairs through all possible channels. When connected to an external load, the PV cell transfers electron in the conduction band to valence band through the load, effectively generating a current flow in an

opposite direction as the current generated by a TR cell. More detailed description and analysis of the physical picture, as well as the mathematical model of the TR cell were given in previous papers [1, 11].

The generated current density from the TR cell is given by the elementary charge $q(> 0)$ times the net flux of photons absorbed by the cell $\dot{N}(T_c, \Delta\mu; T_a)$.

$$I(\Delta\mu) = q\dot{N}(T_c, \Delta\mu; T_s) = q \int_{\omega_g}^{\infty} \frac{d\omega}{2\pi} \varepsilon_{c,a}(\omega) [\Theta(\omega; T_a, 0) - \Theta(\omega; T_c, \Delta\mu)], \quad (1)$$

where $\Theta(\omega; T, \mu) = \frac{1}{\exp[(\hbar\omega - \mu)/k_B T] - 1}$ is the generalized Planck distribution of photons at the frequency ω , at a temperature T and a chemical potential μ , with k_B the Boltzmann constant. $\varepsilon_{c,a}(\omega)$ is the integrated transmissivity over all wavevector components between the cell and a heat sink. The generated voltage is $V = \Delta\mu/q$. Therefore the output power density to the load can be calculated as $P_l(\Delta\mu) = VI(\Delta\mu) = \Delta\mu \cdot \dot{N}(T_c, \Delta\mu; T_a)$.

Similarly, the net radiation power absorbed by the cell can be calculated as

$$P_c(T_c, \Delta\mu; T_a) = \int_0^{\infty} \frac{d\omega}{2\pi} \hbar\omega \cdot \varepsilon_{c,a}(\omega) [\Theta(\omega; T_a, 0) - \Theta(\omega; T_c, \Delta\mu)]. \quad (2)$$

We point out that both the net flux of photons \dot{N} and the radiation P_c to the cell are negative, since more photons are emitted. Hence the efficiency of the TR cell, calculated by $\eta_{TR} = P_l/(P_l - P_c)$ is always smaller than one. Also in examples discussed in this work, the integrated transmissivity below ω_g is zero, so the lower bound of the integral is ω_g in following calculations.

Note that in this model, we assume that the TR cell is ideal, meaning that the only process contributes to the loss of e-h pairs is radiative recombination, as required by the detailed balance. Non-radiative processes such as Auger and surface defect processes are not included for simplification. Therefore, our calculated output power is the maximum power that the TR cell can

generate.

NEAR-FIELD COUPLED TR DEVICE

From the above analysis and equations 1 and 2, we can see that with given thermodynamic parameters (temperatures T_c and T_a , and chemical potential $\Delta\mu$), the performance of a TR device depends only on the transmissivity between the TR cell and the heat sink, which is defined as

$$\varepsilon_{c,a}(\omega) = 2 \times \frac{1}{(2\pi)^2} \int \varepsilon_{c,a}(\omega, \mathbf{K}) d^2\mathbf{K}, \quad (3)$$

which is an integration to the optical transmission coefficient of all possible in-plane wavevector component \mathbf{K} . The transmissivity depends on the optical properties of materials and the geometrical parameters. When the two objects are far away, only propagating wavevector components $|\mathbf{K}| = k < \omega/c$ contribute to the transmissivity, and the upper bound of radiation power is black-body limit. When the distance between the two objects is smaller than the photon wavelength, evanescent wavevector components also contribute to the integrated transmissivity due to photon tunneling [18]. Furthermore, when surface resonances are supported in the system, strong resonant coupling in the near-field can reshape the radiation spectrum, and enhance the integrated transmissivity by several orders at frequencies close to the resonances [19–21]. Based on this principle, near-field radiative heat transfer has been widely studied and applied to near-field TPV system designs [10, 22–25], and recently to TR device designs [4, 11].

For a given material, the dispersion of its dielectric function, which determines the surface resonant mode, is an intrinsic property. Insulating materials with dielectric function described by a Lorentz model support surface phonon polaritons; metallic materials with dielectric function

described by a Drude model support surface plasmon polaritons. In order to maximize the radiative transfer, the resonant mode needs to be close to and slightly larger than the bandgap frequency ω_g . However, the surface resonant frequencies of natural materials, especially the SPP mode frequency supported by metallic materials, are often much higher than the small ω_g of cells used for thermoradiative power conversion.

We show that nanostructured materials can support additional surface resonances that are closer to ω_g , and, when placed close to the TR cell, can enhance the near-field coupling and the radiative transfer. Therefore the energy conversion can be done more rapidly, and higher power density can be achieved with the same TR cell.

For the following calculations, we use a TR cell with bandgap energy $E_g = 0.3$ eV, which corresponds to the bandgap of InAs [26] and bulk Black Phosphorous [27, 28]. The dielectric function of the TR cell is governed by the direct valence-to-conduction interband transition [29, 30], and is described by $\epsilon_{cell}(\omega) = \epsilon_r(\omega) + i\epsilon_i(\omega)$, where

$$\epsilon_i(\omega) = \begin{cases} A \sqrt{x-1}/x^2, & x > 1 \\ 0, & x < 1 \end{cases} \quad (4)$$

$$\epsilon_r(\omega) = \begin{cases} B + A(2 - \sqrt{1+x})/x^2, & x > 1 \\ B + A(2 - \sqrt{1+x} - \sqrt{1-x})/x^2, & x < 1 \end{cases}$$

with $x = \hbar\omega/E_g$, $A = 9$, and $B = 10$.

For the metallic heat sink, the dielectric function is approximated by the Drude model:

$$\epsilon_m = 1 - \frac{\omega_p^2}{\omega^2 + i\gamma\omega}. \quad (5)$$

where ω_p is the plasma frequency, γ is the damping rate, and the resonant frequency of SPP is

given by $\omega_{SPP} = \omega_p / \sqrt{2}$. The parameters will be given in the following calculations for each configuration. Note that in the model of this work, the temperatures of the cell and the heat sink are assumed to be constant. Therefore, the temperature dependency of the optical properties of the materials used in the model is not considered.

The integrated transmissivity and radiative transfer of a system involves grating structures can be calculated based on the scattering theory [31, 32] in combination with the rigorous coupled-wave analysis (RCWA) method [33, 34]. Assume the structure is periodic along x -direction with periodicity p , infinitely long in y -direction, and the TR cell and the grating are separated by a distance d in z -direction, the frequency-dependent integrated transmissivity $\varepsilon_{c,a}(\omega)$ is obtained by integrating wavevector-dependent components $\varepsilon_{c,a}(\omega, k_x, k_y)$ over wavevectors in the x -direction (k_x) and y -direction (k_y), with the integration limit on k_x restricted to the first Brillouin zone defined by the periodicity in the x -direction. Furthermore, the contributions from the positive and negative halves of the Brillouin zone is identical due to the inversion symmetry, therefore we can obtain the integrated transmissivity by Eq. 6.

$$\varepsilon_{c,a}(\omega) = \frac{1}{2\pi^2} \int_{-\infty}^{\infty} \int_{-\pi/p}^{\pi/p} \varepsilon_{c,a}(\omega, k_x, k_y) dk_x dk_y = \frac{2}{\pi^2} \int_0^{\infty} \int_0^{\pi/p} \varepsilon_{c,a}(\omega, k_x, k_y) dk_x dk_y \quad (6)$$

The wavevector-dependent transmissivity components $\varepsilon_{c,a}(\omega, k_x, k_y)$ can be formulated with scattering theory [33], and the required scattering matrix between the TR cell and the heat sink is obtained via RCWA calculation [33, 34]. The reflection coefficient matrices for both surfaces are of dimensions $2(2N + 1)$, where N is the maximum diffraction order considered [35]. To obtain accurate results within reasonable computation time, we use $N = 35$ in the RCWA calculation. The wavevector component k_x is linearly discretized into 21 values between 0 and π/p , and the

k_y component is linearly discretized into 81 values between 0 and maximum value of $100\omega/c$. The computation time is about 15 hours on a personal computer with Intel Core i5-5300U CPU. We have verified that with these settings the numerical error due to discretization is very low. Doubling the discretization gives a difference in obtained integrated transmissivity of less than 1%.

RESULTS AND DISCUSSION

We first consider a heat sink with a metallic material of lower plasma frequency. The dielectric function of ZrC can be fitted with the Drude model as described by Eq. 5, and the plasma frequency is $\omega_p = 1.29 \times 10^{15}$ rad/s, with damping rate approximately $\gamma = 2.58 \times 10^{12}$ rad/s. Therefore the SPP frequency of ZrC ω_{SPP} is at 0.6 eV [10, 36], which is about 2 times of the frequency corresponding to the bandgap ω_g . We first consider a planar system with a gap of $d = 10$ nm between the TR cell and the ZrC heat sink, as shown in Fig. 1(a). The integrated transmissivity spectrum is calculated and plotted as the blue curve in Fig. 2(a). As expected, a sharp peak is observed at 2 times of ω_g . As a reference, the integrated transmissivity of the TR cell to a blackbody is plotted as the dashed black curve in the same figure. It is seen that in the frequency band of interest, the integrated transmissivity due to the near-field coupling to the planar heat sink can indeed exceed the integrated transmissivity to an ideal blackbody. For the near-field coupled system, $\varepsilon_{c,a}(\omega)$ is calculated with RCWA method for the frequency range from ω_g to $3\omega_g$ with $0.01\omega_g$ spacing. In this system configuration, over 99% of power conversion is due to radiation between ω_g and $2.5\omega_g$; we have also verified that doubling the number of frequency points gives a difference in power output of less than 1%.

Then we calculate the integrated transmissivity when a grating structure is added to the surface of the heat sink, as shown in Fig. 1(b). The geometrical parameters for the gratings are $h = 60$ nm, $w = 30$ nm, and $p = 60$ nm. The result is shown in the red curve in Fig. 2(a), where multiple resonance peaks are observed. Due to the periodicity, the SPP mode on the metal surface is truncated and folded into multiple bands within the Brillouin zone, and the peaks in the integrated transmissivity spectrum correspond to different order of modes. This can be verified with mode profiles, and shown in Fig. 2(b)-(d) with three different resonant modes. The mode profiles are obtained with eigenvalue solver in COMSOL [37], which is a finite-element method based commercial software for full-wave simulations. In the simulations, periodic boundary conditions are applied to the left and right end of the structure as shown in Fig.2(b), and Floquet condition is used to specify the wavevector component k_x and k_y . Absorbing boundary conditions are applied to the top and bottom of the structure. Eigenvalue solver within the RF module is used to find the eigenmodes and associated eigenfrequencies. We have validated the accuracy of the COMSOL simulation model by calculating the SPP mode frequency supported on a metal surface and comparing it with theoretical value, and the numerical error is less than 1%. With this setup, the solver can find all resonant modes associated with the grating structured configuration, including those modes corresponding the enhancement of the near-field radiative transfer.

Next we calculate the generated power density and efficiency of the TR cell based on equations 1 and 2. When the temperature of the TR cell is at $T_c = 1000$ K, and the heat sink is maintained at $T_a = 300$ K, the power density and efficiency of systems with a blackbody heat sink, the near-field coupled planar heat sink, and the near-field coupled grating heat sink are plotted in Fig. 3(a) and (b). For the planar case, the maximum power density is 6.53×10^4 W/m² grating

heat sink, the maximum power density is $9.93 \times 10^4 \text{ W/m}^2$, 48.3 times higher than the blackbody heat sink, and 1.5 times higher than the planar heat sink. The maximum achievable efficiency is all above 60%, which is close to the Carnot efficiency of 70%, as calculated by $(1 - T_a/T_c)$. As mentioned by previous analysis [1, 11], the chemical potential for maximum power density and maximum efficiency are very different. As we can see from the figure, the power output at maximum efficiency point is very little. So the maximum power density is a better merit to evaluate the performance of the TR cell. The chemical potential can be controlled by the cell voltage V , which can be adjusted by the load resistance, in order to achieve the maximum power output.

When the temperature of the TR cell is at a lower $T_c = 500 \text{ K}$, while the heat sink is still maintained at $T_a = 300 \text{ K}$, the power density and efficiency are calculated similarly and plotted in Fig. 3(c) and (d). The peak efficiency is again close to the Carnot efficiency, which is now 40%. The peak generated power density is 11.7, 159.3, and 453.4 W/m^2 , for the case of blackbody, planar, and grating heat sink, respectively. Due to the much lower source temperature, the generated power density is two orders lower than the system at $T_c = 1000 \text{ K}$. However, the near-field coupled heat sink with grating has a more significant enhancement of output power density, at 2.9 times higher than the planar structure.

With resonant modes designed by the geometries of nanostructures, the material selection for the heat sink can be more flexible, and even noble metals with much higher plasma frequency can be used. Next, we study a TR cell coupled to a gold heat sink. Fitted by a Drude model [16], the plasma frequency of gold is $\omega_p = 1.37 \times 10^{16} \text{ rad/s}$, with damping rate $\gamma = 7.31 \times 10^{13} \text{ rad/s}$. The SPP resonant frequency on a planar gold surface, $\omega_{SPP} = \omega_p / \sqrt{2}$, is at $8.98 \times 10^{15} \text{ rad/s}$, corresponding to an energy of 6.4 eV, which is over 21 times higher than the TR cell bandgap

energy of 0.3 eV.

With a planar gold surface coupled to the same TR cell at a distance of 10 nm away, the integrated transmissivity is calculated and plotted together with the blackbody reference in Fig. 4(a). As the SPP resonance is far away from the plotted frequency range, the integrated transmissivity is lower than the blackbody reference. A grating structure can also be fabricated on the gold surface, as shown in Fig. 1(b). We choose $h = 500$ nm, $w = 50$ nm, and $p = 100$ nm for the gold grating, and calculate the integrated transmissivity of the system again. As shown in Fig. 4(a), the integrated transmissivity is plotted for all three cases with frequency range between ω_g and $4\omega_g$. We have verified that the radiation in this frequency range contributes to over 99.5% of the power conversion and contributions with frequency above the range is negligible. The calculated transmissivity with the grating structure is higher than the planar counterpart and the blackbody reference in the frequency range, with multiple resonant peaks. These peaks are due to the cavity modes corresponds to different wavevector components. The resonant modes are calculated with COMSOL, and the mode profiles when $k_x = \pi/p$ and $k_y = 0$ are shown in Fig. 4(b) and (c). As indicated by the magnetic field distribution, these are cavity modes confined in the narrow metal slit, and couple to the external field through the open end of the slit. The mode shown in Fig. 4(b) is the fundamental mode and the mode shown in Fig. 4(c) is the second order cavity mode.

The calculated power density and efficiency are plotted in Fig. 5 for temperature $T_c = 1000$ K and $T_c = 500$ K respectively, with temperature at the heat sink kept at $T_a = 300$ K in both cases. Due to the poor mismatch between the SPP resonance of planar gold surface and the TR cell bandgap, the generated power density is lower than the system with an ideal blackbody heat sink. However, with the grating heat sink, the generated power density exceeds the system with an

ideal blackbody heat sink by 3.6 times at $T_c = 1000$ K, and 3.9 times at $T_c = 500$ K.

Comparing Fig. 3 and Fig. 5, we also notice that the power density with the second grating design (Fig. 5(a)) is one order smaller than the first (Fig. 3(a)) at the same operating temperature. This is due to the fact that more photons with energy closer to the bandgap are transmitted in the first design, and can be seen from the integrated transmissivity curves in Fig. 2(a) and Fig. 4(a). However, for the second example, the grating structure still helps the system to enhance the output power to a level exceeds the ideal blackbody reference.

Note that in the above calculation, we assumed the TR cell to be ideal, where only radiative recombination process is considered. Non-radiative loss mechanisms, such as Auger and surface defect processes, were not included in the model. On the one hand, including the loss terms will reduce the expected output power; on the other hand, these processes have similar impact on the systems operating at the same temperature, regardless of the heat sink design. Therefore although the absolute numbers of power density will be smaller, the ratio of output power between different heat sink designs is expected to be about the same [4].

CONCLUSIONS

In conclusion, we examined how the nano-grating structure on the heat sink can increase the TR performance. The performance of the TR can be greatly enhanced with near-field coupling, which occurs by placing a heat sink in close proximity with the cell. Heat sinks supporting surface resonant modes that are close in energy to the bandgap energy of the TR cell are able to boost the radiative transfer of photons and eventually the electric power generation. Metals with dielectric functions described by a Drude model support surface plasmon polaritons, and typically have

large thermal conductivities. Therefore they are good candidates for heat sink of a TR device. However, most metallic materials have surface resonant frequencies much higher in energy than the TR cell bandgap. The mismatch can be addressed with nanostructured surfaces. We show that grating structures support additional surface modes such as truncated surface plasmons and cavity modes depending on the material and geometry. Two grating designs for a TR device were analyzed and calculated, and the performances were compared with planar structures and a blackbody reference. In both designs, the grating structure has a significantly better output power density than the planar and blackbody case. With these findings, we are able to overcome the mismatch in energy of surface resonance and the TR cell bandgap, and use materials such as noble metals as the near-field heat sink of the TR device, for better heat dissipation and enhanced power generation.

-
- [1] R. Strandberg, *Journal of Applied Physics* **117**, 055105 (2015), <http://dx.doi.org/10.1063/1.4907392>,
URL <http://dx.doi.org/10.1063/1.4907392>.
- [2] R. Strandberg, *Journal of Applied Physics* **118**, 215102 (2015), <http://dx.doi.org/10.1063/1.4936614>,
URL <http://dx.doi.org/10.1063/1.4936614>.
- [3] P. Santhanam and S. Fan, *Phys. Rev. B* **93**, 161410 (2016), URL <http://link.aps.org/doi/10.1103/PhysRevB.93.161410>.
- [4] W.-C. Hsu, J. K. Tong, B. Liao, Y. Huang, S. V. Boriskina, and G. Chen, *Scientific Reports* **6**, 34837 EP (2016), article, URL <http://dx.doi.org/10.1038/srep34837>.
- [5] Y. X. Yeng, W. R. Chan, V. Rinnerbauer, V. Stelmakh, J. J. Senkevich, J. D. Joannopoulos, M. Soljacic, and I. Čelanović, *Opt. Express* **23**, A157 (2015), URL <http://www.opticsexpress.org/abstract.cfm?URI=oe-23-3-A157>.
- [6] H. Sai and H. Yugami, *Applied Physics Letters* **85**, 3399 (2004), URL <http://scitation.aip.org/content/aip/journal/apl/85/16/10.1063/1.1807031>.
- [7] N. Nguyen-Huu, J. PiÅtóra, and M. Cada, *Nanotechnology* **27**, 155402 (2016), URL <http://stacks.iop.org/0957-4484/27/i=15/a=155402>.
- [8] B. J. Lee, L. P. Wang, and Z. M. Zhang, *Opt. Express* **16**, 11328 (2008), URL <http://www.opticsexpress.org/abstract.cfm?URI=oe-16-15-11328>.
- [9] P. Würfel and U. Würfel, *Physics of Solar Cells: From Basic Principles to Advanced Concepts*, Physics textbook (Wiley, 2009), ISBN 9783527408573, URL <https://books.google.com/>

books?id=w6Ii4r7FuskC.

- [10] A. Karalis and J. Joannopoulos, *Scientific Reports* **6**, 28472 (- 2016/07/01/online).
- [11] C. Lin, B. Wang, K. H. Teo, and Z. Zhang, under review (2017).
- [12] L. Zhu, S. Sandhu, C. Otey, S. Fan, M. B. Sinclair, and T. Shan Luk, *Applied Physics Letters* **102**, 103104 (2013), URL <http://scitation.aip.org/content/aip/journal/apl/102/10/10.1063/1.4794981>.
- [13] H. Chalabi, E. Hasman, and M. L. Brongersma, *Opt. Express* **22**, 30032 (2014), URL <http://www.opticsexpress.org/abstract.cfm?URI=oe-22-24-30032>.
- [14] A. Karalis and J. D. Joannopoulos, *Applied Physics Letters* **107**, 141108 (2015), URL <http://scitation.aip.org/content/aip/journal/apl/107/14/10.1063/1.4932520>.
- [15] C. Lin, B. Wang, K. H. Teo, and P. Bandaru, under review (2017).
- [16] P. B. Johnson and R. W. Christy, *Phys. Rev. B* **6**, 4370 (1972), URL <http://link.aps.org/doi/10.1103/PhysRevB.6.4370>.
- [17] P. S. Davids, F. Intravaia, and D. Dalvit, *Opt. Express* **22**, 12424 (2014), URL <http://www.opticsexpress.org/abstract.cfm?URI=oe-22-10-12424>.
- [18] D. Polder and M. Van Hove, *Phys. Rev. B* **4**, 3303 (1971), URL <http://link.aps.org/doi/10.1103/PhysRevB.4.3303>.
- [19] A. Narayanaswamy and G. Chen, *Applied Physics Letters* **82**, 3544 (2003), URL <http://scitation.aip.org/content/aip/journal/apl/82/20/10.1063/1.1575936>.
- [20] K. Joulain, J.-P. Mulet, F. Marquier, R. Carminati, and J.-J. Greffet, *Surface Science Reports* **57**, 59 (2005), ISSN 0167-5729, URL <http://www.sciencedirect.com/science/article/pii/>

S0167572905000105.

- [21] E. Rousseau, A. Siria, G. Jourdan, S. Volz, F. Comin, J. Chevrier, and J.-J. Greffet, *Nat Photon* **3**, 514 (2009), ISSN 1749-4885, URL <http://dx.doi.org/10.1038/nphoton.2009.144>.
- [22] O. Ilic, M. Jablan, J. D. Joannopoulos, I. Celanovic, and M. Soljačić, *Opt. Express* **20**, A366 (2012), URL <http://www.opticsexpress.org/abstract.cfm?URI=oe-20-103-A366>.
- [23] X. Liu and Z. Zhang, *ACS Photonics* **2**, 1320 (2015), URL <http://dx.doi.org/10.1021/acsp Photonics.5b00298>.
- [24] X. Liu, L. Wang, and Z. M. Zhang, *Nanoscale and Microscale Thermophysical Engineering* **19**, 98 (2015), URL <http://dx.doi.org/10.1080/15567265.2015.1027836>.
- [25] S. Jin, M. Lim, S. S. Lee, and B. J. Lee, *Opt. Express* **24**, A635 (2016), URL <http://www.opticsexpress.org/abstract.cfm?URI=oe-24-6-A635>.
- [26] S. Adachi, *Journal of Applied Physics* **66**, 6030 (1989), <http://dx.doi.org/10.1063/1.343580>, URL <http://dx.doi.org/10.1063/1.343580>.
- [27] C. D. Zhang, J. C. Lian, W. Yi, Y. H. Jiang, L. W. Liu, H. Hu, W. D. Xiao, S. X. Du, L. L. Sun, and H. J. Gao, *The Journal of Physical Chemistry C* **113**, 18823 (2009), <http://dx.doi.org/10.1021/jp907062n>, URL <http://dx.doi.org/10.1021/jp907062n>.
- [28] A. Castellanos-Gomez, *The Journal of Physical Chemistry Letters* **6**, 4280 (2015), pMID: 26600394, <http://dx.doi.org/10.1021/acs.jpcllett.5b01686>, URL <http://dx.doi.org/10.1021/acs.jpcllett.5b01686>.
- [29] D. E. Aspnes and A. A. Studna, *Phys. Rev. B* **27**, 985 (1983), URL <http://link.aps.org/doi/10.1103/PhysRevB.27.985>.

- [30] S. Adachi, Phys. Rev. B **35**, 7454 (1987), URL <http://link.aps.org/doi/10.1103/PhysRevB.35.7454>.
- [31] J. Lussange, R. Gu erout, F. S. S. Rosa, J.-J. Greffet, A. Lambrecht, and S. Reynaud, Phys. Rev. B **86**, 085432 (2012), URL <http://link.aps.org/doi/10.1103/PhysRevB.86.085432>.
- [32] X. L. Liu and Z. M. Zhang, Applied Physics Letters **104**, 251911 (2014), <http://aip.scitation.org/doi/pdf/10.1063/1.4885396>, URL <http://aip.scitation.org/doi/abs/10.1063/1.4885396>.
- [33] M. G. Moharam, T. K. Gaylord, E. B. Grann, and D. A. Pommet, J. Opt. Soc. Am. A **12**, 1068 (1995), URL <http://josaa.osa.org/abstract.cfm?URI=josaa-12-5-1068>.
- [34] L. Li, J. Opt. Soc. Am. A **13**, 1870 (1996), URL <http://josaa.osa.org/abstract.cfm?URI=josaa-13-9-1870>.
- [35] J. I. Watjen, X. L. Liu, B. Zhao, and Z. M. Zhang, Journal of Heat Transfer **139**, 052704 (2017), ISSN 0022-1481, URL <http://dx.doi.org/10.1115/1.4035356>.
- [36] F. A. Modine, T. W. Haywood, and C. Y. Allison, Phys. Rev. B **32**, 7743 (1985), URL <http://link.aps.org/doi/10.1103/PhysRevB.32.7743>.
- [37] (????), URL <http://www.comsol.com/>.

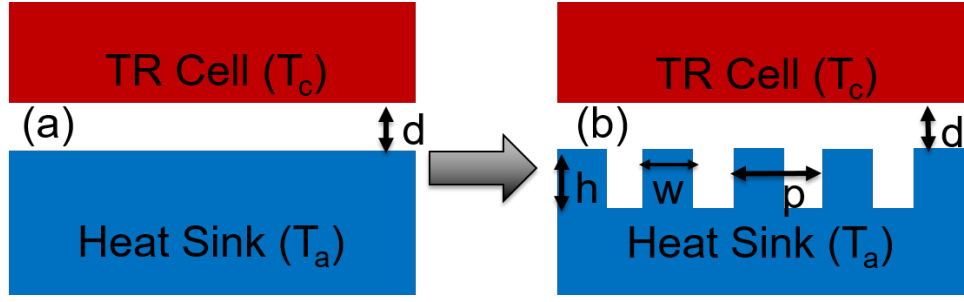


FIG. 1: Structures of near-field TR device (a) with planar heat sink, and (b) with periodically structured heat sink.

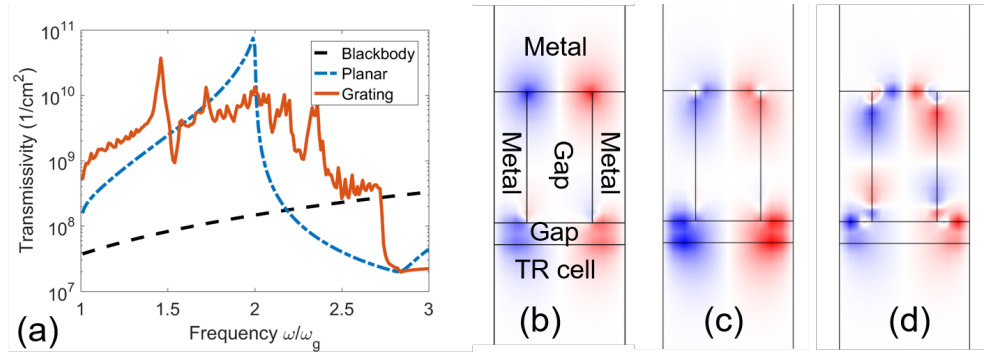


FIG. 2: (a) Calculated integrated transmissivity as a function of frequency for three systems: TR cell with ideal blackbody heat sink, TR cell coupled with planar metallic heat sink, TR cell coupled with metallic grating heat sink. The metal is ZrC, with with $h = 60$ nm, $w = 30$ nm, and $p = 60$ nm. Magnetic field distribution of resonant modes supported by the system when $k_x = 0$ and $k_y = 0$, at normalized frequency ω/ω_g of (b) 1.50, (c) 1.83 and (d) 1.99.

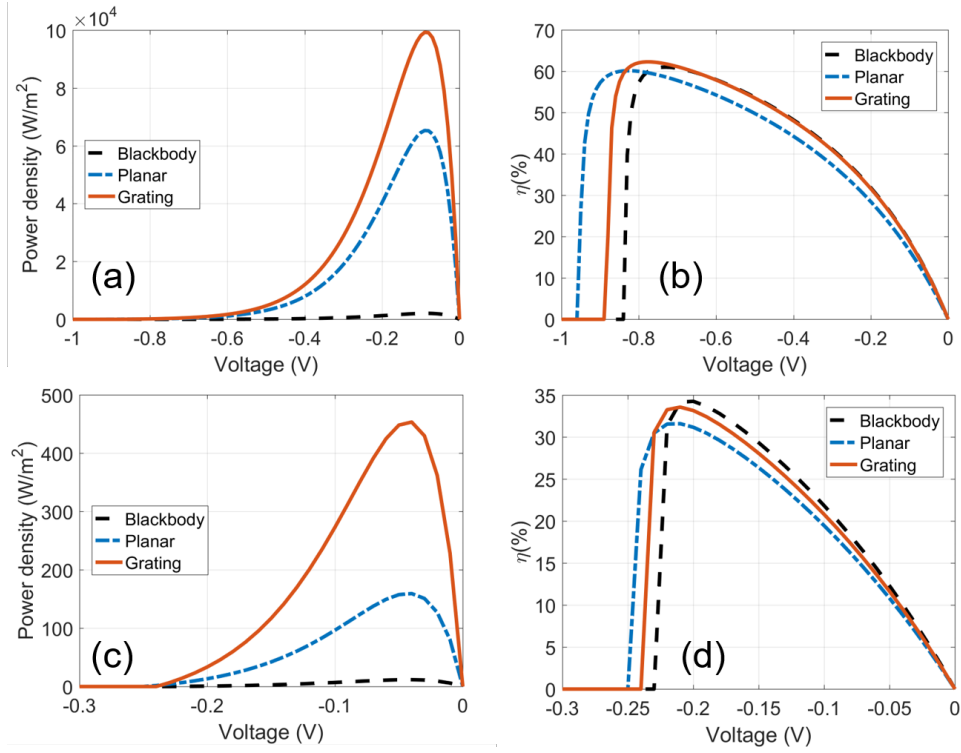


FIG. 3: The calculated (a) power density and (b) efficiency for the three systems corresponds to Fig. 2 when the cell is at $T_c = 1000$ K, and the heat sink is at $T_a = 300$ K. The (c) power density and (d) efficiency for the three systems are also shown when the cell is at $T_c = 500$ K, and the heat sink is at $T_a = 300$ K.

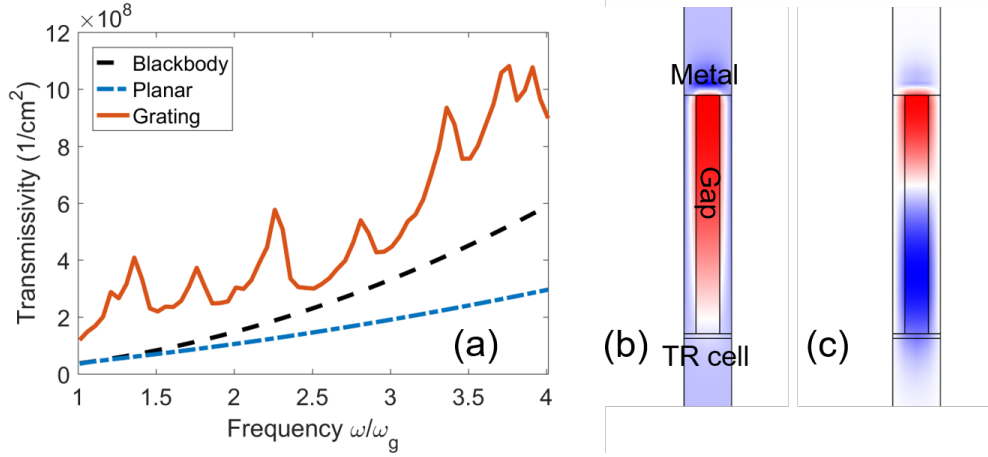


FIG. 4: (a) Calculated integrated transmissivity as a function of frequency for three systems: TR cell with ideal blackbody heat sink, TR cell coupled with planar metallic heat sink, TR cell coupled with metallic grating heat sink. The metal is gold, with $h = 500$ nm, $w = 50$ nm, and $p = 100$ nm. Magnetic field distribution of resonant modes supported by the system when $k_x = \pi/p$ and $k_y = 0$, at normalized frequency ω/ω_g of (b) 1.23, and (c) 3.55.

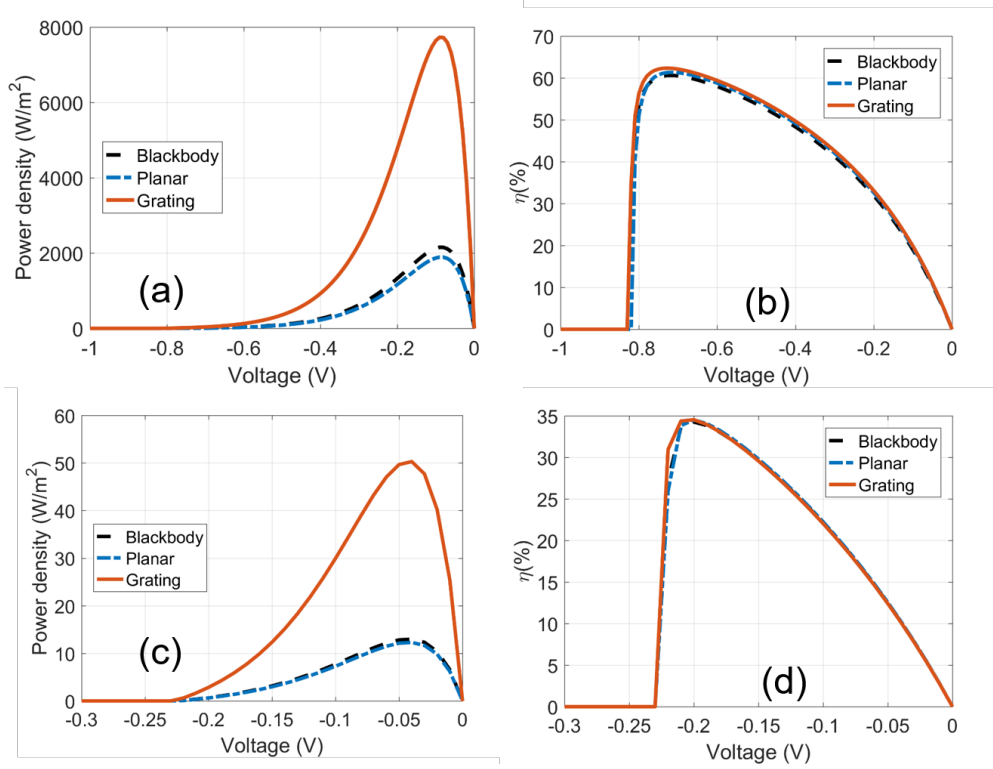


FIG. 5: The calculated (a) power density and (b) efficiency for the three systems corresponds to Fig. 4 when the cell is at $T_c = 1000$ K, and the heat sink is at $T_a = 300$ K. The (c) power density and (d) efficiency for the three systems are also shown when the cell is at $T_c = 500$ K, and the heat sink is at $T_a = 300$ K.